Advances in Engineering Software 102 (2016) 1–13

Contents lists available at ScienceDirect

Advances in Engineering Software

journal homepage: www.elsevier.com/locate/advengsoft

Research paper

A fast uncertainty analysis for material nonlinear problems based on reanalysis and semi-analytic strategy

Guanxin Huang[a], Hu Wang[a,*], Lei Chen[a], Enying Li[b,*], Guangyao Li[a]

[a] State Key Laboratory of Advanced Design and Manufacturing for Vehicle Body, Hunan University, Changsha, 410082, PR China
[b] School of Logistics, Central South University of Forestry and Teleology, Changsha, 41004, PR China

ARTICLE INFO

Article history:
Received 1 April 2016
Revised 17 July 2016
Accepted 14 August 2016

Keywords:
Interval model
Semi-analytic uncertainty analysis
Pseudo elastic analysis
Combined approximation

ABSTRACT

A novel semi-analytic method for interval-based uncertainty analysis is suggested to calculate the uncertainty measure index in this study. As nonlinear problems commonly cannot be solved analytically, an analytic interval-based uncertainty analysis method for linear problems is deduced, and an explicit expression of the measure index of uncertainty is given. To extend this form to nonlinear analysis, a semi-analytic uncertainty analysis (SAUA) method is suggested by integrating gradient-based optimization methods and Taylor expansion. Initially, a pseudo optimal solution is obtained. Sequentially, a Taylor expansion is used to calculate the performance function based on the pseudo optimal solution. In this way, the uncertainty measure index can be obtained analytically. Considering the bottleneck of surrogate model, an efficient reanalysis assisted material nonlinear analysis (RAMNA) method is integrated. Thus, the efficiency and accuracy of the suggested method are both enhanced. The SAUA method has been applied to large-scale reliability analysis of vehicle components. The results show that the SAUA is effective and efficient, especially for large-scale problems. Furthermore, the SAUA method can also be extended for other mechanical design, and contribute to shortening the design period.

1. Introduction

Material nonlinear analysis is an important research area of structure design. Generally, material nonlinear analysis is an iterative process with large scale simulations. Therefore, the efficiency is an important property of material nonlinear analysis methods. When uncertainty occurs in material nonlinear problems, the situation will become even more severe.

For uncertain analysis, the most popular methods are based on probability theories. These methods are mainly described in two kinds of models: stochastic and fuzzy models. Generally, the distribution of stochastic variables should be given or assumed. In practice, the distribution is usually derived from experiments or prior information. Due to the booming of probability theories, the stochastic models are well developed and have been used in multidisciplines [1–4]. The uncertainty formulized using stochastic models is also known as 'reliability'. In stochastic models, Monte–Carlo simulation (MCS) [5] is one of the most popular methods. It achieves accurate solution regardless of dimension of problems [6,7]. The major bottleneck is that the MCS requires a large number of samples to achieve the reliability index. Therefore, many applications of MCS are based on surrogates. Besides MCS, stochastic finite element (SFE) [4,8] is also a useful tool in structural reliability analysis. Compared to stochastic models, fuzzy models pay more attention on subjective probability. The fuzzy theory was initially used for mathematical programming problems [9,10]. Then, it was introduced for uncertainty analysis [11–14]. Similarly, the major bottleneck of fuzzy-based methods is also expensive computational cost. To overcome this challenge, convex models are developed [15].

Convex models form a convex set of functions or vectors, and the uncertainties of system or structure can be represented by examining the failure function on the convex. The applications of convex model in structure analysis can be found in many studies [16–18]. As a special case of convex models, the interval model, because of its concise description of theory and low requirement of input information, has attracted more and more attentions. Qiu and Elishakoff developed an interval analysis method for anti-optimization of structures with large uncertain-but-non-random parameters [19]. Sengupta et al. defined a satisfactory crisp equivalent system of an inequality constraint with interval coefficients [20], and the system was solved via an interval linear programming method. Guo and Lü proposed a static linear interval finite element method (IFEM) by combining interval analysis and FEM to solve the non-random uncertain structures [21]. Jiang et al.

* Corresponding author. Fax: +86 0731 88822051.
E-mail addresses: wanghu@hnu.edu.cn, wanghuenying@hotmail.com (H. Wang), enyasteven@hotmail.com (E. Li).

http://dx.doi.org/10.1016/j.advengsoft.2016.08.008
0965-9978/

suggested an optimization method for uncertain structures using interval analysis as an extension of convex models [22]. Then the method is applied to U-shaped forming [23] and composite laminated plate [24] uncertainty analysis. Jiang et al. also presented a sequential nonlinear interval number programming (SNINP) method to deal with uncertain optimizations [25]. Wu et al. proposed an interval uncertainty analysis method for multi-body dynamics of mechanical systems based on Chebyshev inclusion functions [26]. Li et al. proposed an uncertain multi-objective multidisciplinary design optimization methodology by formulating the design as a nested three-loop optimization [27].

Generally, uncertainty problems are usually analyzed via large amount of evaluations (simulations). For linear problems, with the increase of complexity and scale of model, the computational cost of uncertain analysis increases in a geometrical progression. The computational cost should be much more expensive when it comes to nonlinear problems due to iterative procedure. Therefore, the efficiency is the key issue for uncertainty analysis of nonlinear problems, especially for real engineering problems. To balance the accuracy and efficiency, a trade-off strategy termed as semi-analytic uncertainty analysis (SAUA), is proposed in this study. To further improve the efficiency, the reanalysis methods are introduced in material nonlinear analysis.

In the research field of reanalysis, several kinds of efficient methods have been proposed for optimization problems. These methods can be mainly divided into two categories: Direct methods (DMs) and approximate methods. DMs are usually suitable for low-rank or local modifications. Most of DMs can obtain an exact solution of the modified structure. As stated by Tuckerman [28], any DM that solves a system by modification of an original model is an explicit or implicit application of the Sherman–Morrison–Woodbury (SMW) formula [29–31]. Cheikh et al. presented a DM based on a Moore Penrose generalized inverse for static reanalysis of structures [32]. Huang and Wang, et al. suggested an Independent coefficients (IC) method for large-scale problems [33]. Song et al. proposed a DM by updating the triangular factorization in sparse matrix solution [34]. Compared with DMs, approximate methods can't obtain an exact solution. However, high-rank or global modifications can usually be well disposed by these kind of algorithms. Combined approximation (CA) [35–37] is one of the most popular approximate reanalysis methods. The CA method is firstly proposed for linear static problems [38], and it has been extended to multidisciplinary. Kirsch and Papalambros presented a reanalysis approach for geometrical changes in structural systems based on the CA method [39]. Rong et al. extended Kirsch's method to a new effective modal reanalysis method for topological modification [40]. Kirsch et al. used CA to overcome the difficulty of repeating eigenproblem solutions for nonlinear dynamic reanalysis [41]. Chen et al. suggested a universal Iterative Combined Approximation (ICA) approach for all types of topological modifications [42]. Gao and Wang, et al. proposed an adaptive time-based global reanalysis (ATGR) for dynamic problems based on CA method [43]. Zhang et al. applied the CA method to probabilistic analysis and reliability-based design optimization of large-scale structures [44]. Zuo et al. integrated the CA and the genetic algorithm (GA) to improve the efficiency of optimization [45] and suggested a sensitivity analysis based on CA and Taylor expansion [46]. Recently, some extended CA methods have been proposed and applied to multidiscipline. For example, Sun et al. suggested an adaptive technique of Kirsch method for structural reanalysis [47]. Zuo et al. developed a hybrid Fox and Kirsch's reduced basis method for structural static reanalysis [48]. Moreover, other approximate reanalysis methods have been developed in recent years. Epsilon-algorithm was presented for both static problems [49] and dynamic problems [50]. Preconditioned conjugate gradient (PCG) method is a classical iterative algorithm. Kirsch et al. introduced this method for structural reanalysis [51], and Wu et al. developed PCG method for both removal of Degrees of Freedom (DOF) and added DOFs [52–57]. A matrix perturbation method was used by Yang et al. for structural modal reanalysis [58,59]. Wu et al. also developed a reanalysis method based on rational approximation for large changes in design variables [60]. Wang et al. integrated several kinds of reanalysis methods and developed an efficiency parallel platform [54–56]. It can be found that the CA and its alternative methods can be utilized for several kinds of complicated problems [35,37]. In this study, we hope use the CA method to improve the analysis efficiency of material nonlinear problems. Under such circumstance, the mesh of a structure keeps fixed, and the nonlinear may appear locally or globally, which can be treated as structural modification on linear work condition. Therefore, the CA can be utilized to improve the efficiency of material nonlinear analysis.

The rest of this paper is organized as follows: In Section 2, an uncertainty analysis method using interval model is briefly introduced. In Section 3, a SAUA method is suggested for general problems. In Section 4, the SAUA method is applied to material nonlinear problems, and an efficient reanalysis assisted material nonlinear analysis (RAMNA) method is proposed. To test performances of the SAUA, several numerical examples are demonstrated in Section 5. Finally, conclusions are given

2. Uncertainty analysis based on interval model

Assume that $\mathbf{x} = \{\mathbf{x}_1, \mathbf{x}_2, \ldots, \mathbf{x}_n\}$ is a set of uncertain factor vector that affects the performance of a structure or a system. It also can be expressed as interval numbers, and $\mathbf{x}_i (i = 1, 2, \ldots, n)$ can be written as

$$\mathbf{x}_i = [x_i^l, x_i^u], \tag{1}$$

where, x_i^l and x_i^u are lower and upper boundary of $\mathbf{x}_i$, respectively. The performance function can be expressed as

$$G_x(\mathbf{x}) = G_x(\mathbf{x}_1, \mathbf{x}_2, \ldots \mathbf{x}_n). \tag{2}$$

$G_x > 0$ indicates that the structure or the system is under safe criterion and works well, and $G_x < 0$ indicates that the structure or the system is under failure criterion. $G_x = 0$ is the limit state surface, which indicates the structure or system works at a limit state.

The interval number can be standardized as

$$\mathbf{x}_i = x_i^c + x_i^w \boldsymbol{\delta}_i, \tag{3}$$

where, $x_i^c = \frac{x_i^l + x_i^u}{2}$ is termed as the midpoint value of x_i, and $x_i^w = \frac{x_i^u - x_i^l}{2}$ denotes the radius. $\boldsymbol{\delta}_i = [-1, 1]$ is a normalized interval number. Therefore, the performance function expressed by using standardized the interval number can be written as

$$G_\delta(\boldsymbol{\delta}) = G_\delta(\boldsymbol{\delta}_1, \boldsymbol{\delta}_2, \ldots, \boldsymbol{\delta}_n). \tag{4}$$

In the space of standardized interval variables, a set of uncertain variables can be regarded as a normalized hypercube. In the hypercube, the distance between any arbitrary points and the origin can be defined as an infinite norm

$$\|\boldsymbol{\delta}\|_\infty = \max\left(|\boldsymbol{\delta}_1|, |\boldsymbol{\delta}_2|, \ldots, |\boldsymbol{\delta}_n|\right). \tag{5}$$

Based on above definition, the boundary of uncertain variables is $\|\boldsymbol{\delta}\|_\infty = 1$. When the hypercube is within the safe region ($G_\delta > 0$), it means the structure or the system is reliable. In this case, the further the hypercube is away from the limit state surface ($G_\delta = 0$), the more reliable the structure or the system is. When a part or whole of the hypercube is within the failure region ($G_\delta < 0$), the structure or the system is unreliable. The limit state surface and different kinds of hypercube are shown in Fig. 1. Therefore, the minimal distance from the origin to the limit state surface can

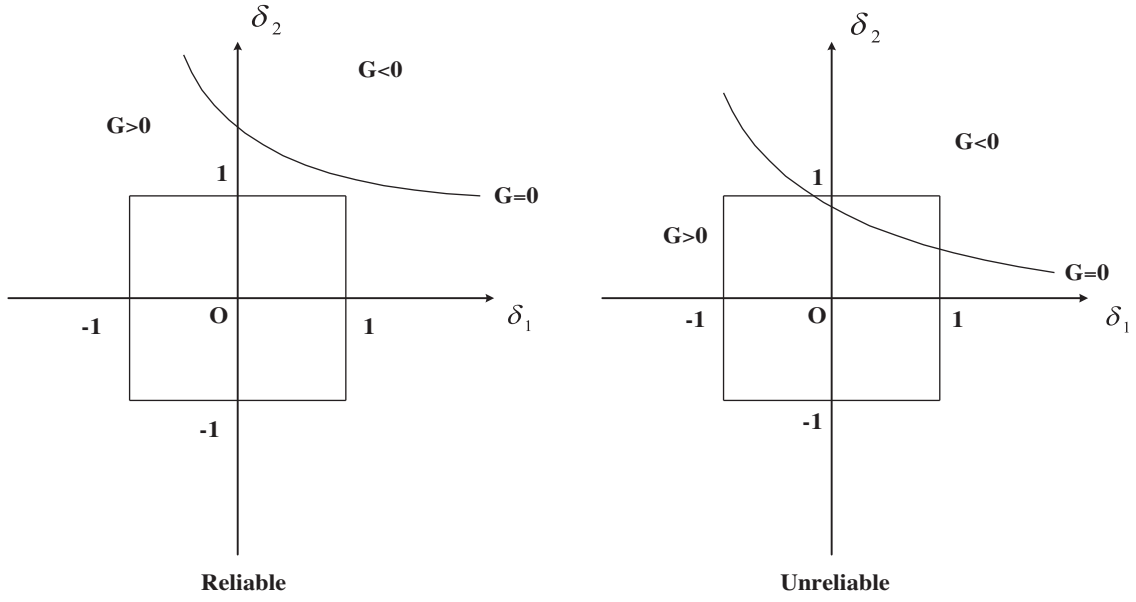

Fig. 1. Limit state surface and range of the interval variables.

be used to indicate the uncertainty of the structure or system. The measure index is defined as

$$\eta = \operatorname{sgn}(G_\delta(0)) \cdot \min_{\boldsymbol{\delta}} \left(\|\boldsymbol{\delta}\|_\infty \right), \quad s.t. \quad G_\delta(\boldsymbol{\delta}) = 0 \tag{6}$$

where $\operatorname{sgn}(\cdot)$ is the sign function.

The mathematical meaning of η is clear: when $\eta > 1$, the structure or system is safe, namely, reliable; when $\eta < -1$, the structure or system is going to fail, namely, unreliable; when $-1 < \eta < 1$, the structure or system might be risk, namely, unreliable.

3. Semi-analytic uncertainty analysis for interval model

For nonlinear analysis, the performance function usually cannot be expressed explicitly by using uncertain variables, thus it is difficult to calculate the uncertainty measure index (Eq. (6)) analytically. Therefore, expensive computation (such as simulation) should be utilized for evaluation. Theoretically, any optimization algorithms, such as gradient based methods, simplex method and heuristic algorithms [61–63], can be used to obtain the uncertainty measure index. However, the number of evaluations is usually tremendous. Therefore, an alternative way to save the computation cost is to use surrogate models [64–69] instead of real evaluations. However, when the surrogate model is used, the error of prediction cannot be avoided due to the fitting model, especially for complicated physical problems. Therefore, the performance of analysis relies heavily on the accuracy of surrogate. For example, for an optimization problem with equality constrains, the optimum obtained by surrogate often does not strictly satisfy the equal constraints. In order to guarantee the accuracy and the efficiency of uncertainty analysis, the SAUA method is suggested in this study.

3.1. Analytic uncertainty analysis for linear problems

Because the formula of uncertainty measure index of nonlinear problems commonly cannot be deduced directly, the uncertainty analysis can be extended from the linear problem which can be explicitly expressed directly. Therefore, a linear analytic uncertainty analysis method is primarily suggested in this section.

For a general linear problem, the performance function can be written as

$$G_\delta(\boldsymbol{\delta}) = \mathbf{a}^T\boldsymbol{\delta} + b. \tag{9}$$

The limit state surface

$$G_\delta(\boldsymbol{\delta}) = \mathbf{a}^T\boldsymbol{\delta} + b = 0 \tag{10}$$

means a hyperplane in the space of $\boldsymbol{\delta}$. The normal direction of the hyperplane is $\mathbf{a}$. Assume that a straight line, which is in normal direction, passes through the origin as shown in Fig. 2, and intersects with the hyperplane Eq. (10) at point $\mathbf{P}$. In this case, $\mathbf{P}$ is the nearest point to the origin on the hyperplane. The straight line mentioned above can be expressed as

$$\boldsymbol{\delta} = k\mathbf{a}, \quad k \in \mathbf{R}, \tag{11}$$

Substitute Eq. (11) into Eq. (10), k can be obtained as

$$k = -\frac{b}{\mathbf{a}^T\mathbf{a}}. \tag{12}$$

Substitute Eq. (12) into Eq. (11), $\mathbf{P}$ can be obtained as

$$\mathbf{P} = k\mathbf{a} = -\frac{b}{\mathbf{a}^T\mathbf{a}}\mathbf{a}. \tag{13}$$

Then, the uncertainty measure index is calculated as

$$\eta = \|\mathbf{P}\|_\infty. \tag{14}$$

The analytic method is summarized in Fig. 2.

As an application, for an elastic stiffness uncertainty analysis, the elasticity modulus and the loads are assumed to be uncertain as

$$\mathbf{E} = E_c + E_w\boldsymbol{\delta}_0 \tag{15}$$

and

$$\mathbf{f}_i = f_i^c + f_i^w\boldsymbol{\delta}_i, \quad (i = 1, 2, \ldots, n). \tag{16}$$

In Eq. (15), E_c is the midpoint value of elasticity modulus $\mathbf{E}$, and E_w is the radius of $\mathbf{E}$. f_i^c and f_i^w are midpoint value and radius of load $\mathbf{f}_i$, respectively. The stiffness measured by the displacement of structure (let's assume it is the displacement of the jth degree of freedom, $u(j)$) should be less than allowable displacement u_s.

In elastic FEA (finite element analysis), the elasticity modulus can be extracted from the stiffness matrix, thus the stiffness matrix corresponding to the midpoint E_c can be given as

$$\mathbf{K}_c = E_c\mathbf{K}_0. \tag{17}$$

where, $\mathbf{K}_c$ is the stiffness matrix when E equals to E_c, and $\mathbf{K}_0$ is the stiffness matrix when E equals to 1.

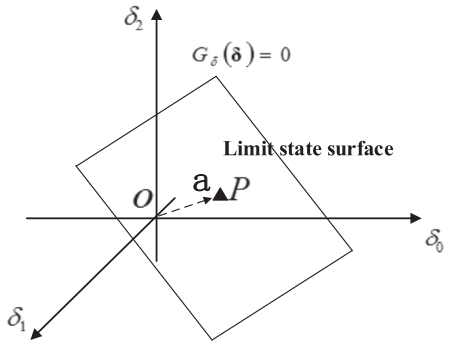

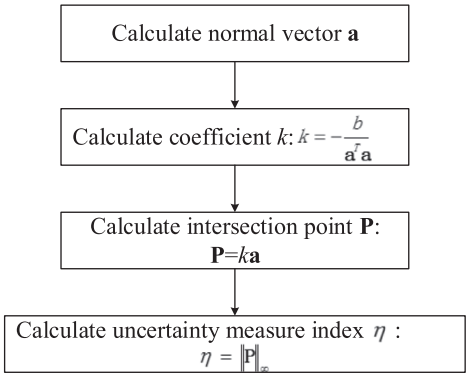

Fig. 2. An illustration of analytical reliability analysis.

Then, the interval stiffness matrix can be given as

$$\mathbf{K} = \left(E_c + E_w\boldsymbol{\delta}_0\right)\mathbf{K}_0 = \left(1 + \frac{E_w}{E_c}\boldsymbol{\delta}_0\right)E_c\mathbf{K}_0 = \left(1 + \frac{E_w}{E_c}\boldsymbol{\delta}_0\right)\mathbf{K}_c. \tag{18}$$

Similarly, the loads can be expressed as

$$\mathbf{f}_i = f_i^c + f_i^w\boldsymbol{\delta}_i = \left(1 + \frac{f_i^w}{f_i^c}\boldsymbol{\delta}_i\right)f_i^c, \quad (i = 1, 2, \ldots, n). \tag{19}$$

Solve the equilibrium equation

$$\mathbf{K}\mathbf{u}_i = \mathbf{f}_i, \tag{20}$$

the displacement can be obtained by Eq. (21) when the ith load is enforced independently.

$$\mathbf{u}_i = \mathbf{K}^{-1}\mathbf{f}_i = \frac{1 + \frac{f_i^w}{f_i^c}\boldsymbol{\delta}_i}{1 + \frac{E_w}{E_c}\boldsymbol{\delta}_0}\mathbf{K}_c^{-1}\mathbf{f}_i^c = \frac{1 + \frac{f_i^w}{f_i^c}\boldsymbol{\delta}_i}{1 + \frac{E_w}{E_c}\boldsymbol{\delta}_0}\mathbf{u}_i^c \tag{21}$$

If all loads are enforced together, the displacement vector can be given as

$$\mathbf{u} = \sum_{i=1}^{n}\mathbf{u}_i = \sum_{i=1}^{n}\frac{1 + \frac{f_i^w}{f_i^c}\boldsymbol{\delta}_i}{1 + \frac{E_w}{E_c}\boldsymbol{\delta}_0}\mathbf{u}_i^c = \sum_{i=1}^{n}\frac{1 + \alpha_i\boldsymbol{\delta}_i}{1 + \beta\boldsymbol{\delta}_0}\mathbf{u}_i^c, \tag{22}$$

where

$$\begin{cases}\alpha_i = \dfrac{f_i^w}{f_i^c} \\ \beta = \dfrac{E_w}{E_c}\end{cases}. \tag{23}$$

According to the stiffness requirement, the performance function can be calculated as

$$G_\delta(\boldsymbol{\delta}) = G_\delta(\boldsymbol{\delta}_0, \boldsymbol{\delta}_1, \ldots, \boldsymbol{\delta}_n) = u_s - \mathbf{u}(j) = u_s - \sum_{i=1}^{n}\frac{1 + \alpha_i\boldsymbol{\delta}_i}{1 + \beta\boldsymbol{\delta}_0}\mathbf{u}_i^c(j). \tag{24}$$

After simplification, the limit state surface is

$$\sum_{i=1}^{n}\alpha_i\mathbf{u}_i^c(j)\boldsymbol{\delta}_i - \beta u_s\boldsymbol{\delta}_0 + \Delta u = 0, \tag{25}$$

where

$$\Delta u = \sum_{i=1}^{n}\mathbf{u}_i^c(j) - u_s, \tag{26}$$

where $\sum_{i=1}^{n}\mathbf{u}_i^c(j)$ is the displacement when all loads work as the midpoint value, termed as $\mathbf{u}_c(j)$.

Eq. (25) represents a hyperplane in a dimension $n+1$ space, and the normal direction of the hyperplane is

$$\mathbf{a} = \left(\frac{\alpha_1\mathbf{u}_1^c(j)}{m}, \frac{\alpha_2\mathbf{u}_2^c(j)}{m}, \cdots, \frac{\alpha_n\mathbf{u}_n^c(j)}{m}, -\frac{\beta u_s}{m}\right), \tag{27}$$

where

$$m = \sqrt{\left(\alpha_1\mathbf{u}_1^c(j)\right)^2 + \left(\alpha_2\mathbf{u}_2^c(j)\right)^2 + \cdots + (\alpha_n\mathbf{u}_n^c(j))^2 + (\beta u_s)^2}. \tag{28}$$

Then the intersection mentioned in Eq. (13) can be obtained as

$$\mathbf{P} = -\frac{\Delta u}{\sum_{i=1}^{n}\frac{\left(\alpha_i\mathbf{u}_i^c(j)\right)^2}{m} + \frac{(\beta u_s)^2}{m}}\mathbf{a}. \tag{29}$$

According to Eq. (14), the uncertainty measure index can be achieved.

3.2. Semi-analytic uncertainty analysis

Generally, the cost for an optimization procedure to find a high-accuracy solution is usually much higher than a low-accuracy one. Based on this assumption, the idea of SAUA method can be described as follows:

(1) For Eq. (6), a pseudo solution $\bar{\boldsymbol{\delta}}$ with a relaxed converge criterion is obtained using any available optimization method (Steepest descent method in present study).
(2) By approximating the performance function with a Taylor expansion, the uncertainty measure index is calculated analytically in the neighborhood of $\bar{\boldsymbol{\delta}}$.

An illustration of the SAUA is shown in Fig. 3.

In the neighborhood of $\bar{\boldsymbol{\delta}}$, the performance function can be approximated by using a Taylor expansion

$$G_\delta(\boldsymbol{\delta}) = G_\delta\left(\bar{\boldsymbol{\delta}}\right) + \nabla G_\delta^T \cdot d\boldsymbol{\delta}, \tag{30}$$

where ∇G is the gradient vector of the performance function. Then Eq. (6) can be transformed to

$$\begin{aligned}&\eta = \operatorname{sgn}(G_\delta(0)) \cdot \min_{d\boldsymbol{\delta}}(\|\bar{\boldsymbol{\delta}} + d\boldsymbol{\delta}\|_\infty) \\ &s.t. \quad G_\delta\left(\bar{\boldsymbol{\delta}}\right) + \nabla G_\delta^T \cdot d\boldsymbol{\delta} = 0\end{aligned}. \tag{31}$$

Because

$$\left\|\bar{\boldsymbol{\delta}} + d\boldsymbol{\delta}\right\|_\infty \le \left\|\bar{\boldsymbol{\delta}}\right\|_\infty + \left\|d\boldsymbol{\delta}\right\|_\infty, \tag{32}$$

the uncertainty measure index can be calculated as

$$\eta = \operatorname{sgn}(G_\delta(0)) \cdot \left\|\bar{\boldsymbol{\delta}} + d\boldsymbol{\delta}^*\right\|_\infty, \tag{33}$$

where $d\boldsymbol{\delta}*$ is the solution of optimization problem

$$\begin{aligned}&\min_{d\boldsymbol{\delta}}\left(\left\|d\boldsymbol{\delta}\right\|_\infty\right) \\ &s.t. \quad G_\delta\left(\bar{\boldsymbol{\delta}}\right) + \nabla G_\delta^T \cdot d\boldsymbol{\delta} = 0\end{aligned}. \tag{34}$$

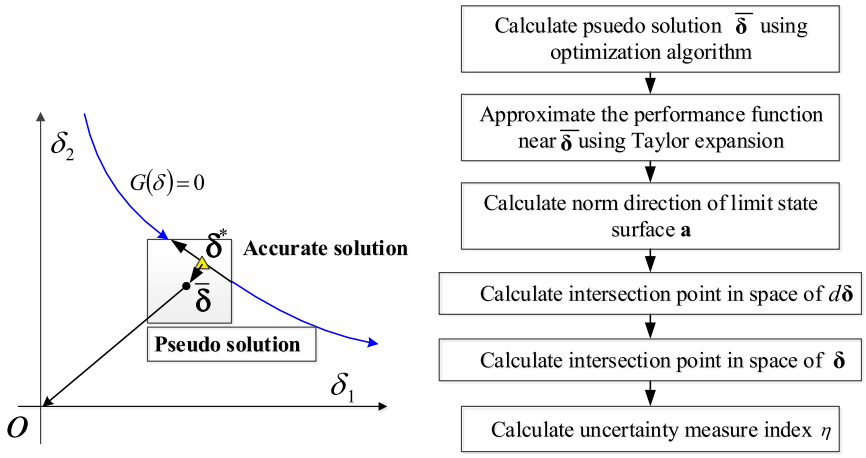

Fig. 3. An illustration of the SAUA method and flowchart.

Eq. (34) means the optimal point is the one which satisfies the constraint equation and is closest to point $\bar{\delta}$.

In the space of $d\delta$, the optimal point is closest to the origin and the constraint equation represents a hyperplane. The normal direction of the hyperplane is

$$\mathbf{a} = \frac{\nabla G_\delta^T}{\|\nabla G_\delta\|}. \tag{35}$$

The straight line, which is along the normal direction and passes through the origin, can be described as

$$d\boldsymbol{\delta} = k\mathbf{a} = k\frac{\nabla G_\delta^T}{\|\nabla G_\delta\|}, k \in \mathbf{R} \tag{36}$$

Substitute Eq. (36) into the constraint equation, k can be written

$$k = -\frac{G_\delta\left(\bar{\boldsymbol{\delta}}\right)\|\nabla G_\delta\|}{\nabla G_\delta^T \nabla G_\delta}. \tag{37}$$

Then, substitute Eq. (37) into Eq. (36), obtains

$$d\boldsymbol{\delta}^* = -\frac{G_\delta\left(\bar{\boldsymbol{\delta}}\right)}{\nabla G_\delta^T \nabla G_\delta}\nabla G_\delta. \tag{38}$$

By substituting Eq. (38) into Eq. (33), the uncertainty measure index is achieved.

The gradient vector is usually unavailable in practice. As a numerical approximation, the difference quotient is used to calculate the gradient vector instead of the partial derivative. Thus, the gradient vector is calculated as

$$\begin{aligned}\nabla G_\delta &= \left[\frac{\partial G_\delta}{\partial \delta_1} \quad \frac{\partial G_\delta}{\partial \delta_2} \quad \cdots \quad \frac{\partial G_\delta}{\partial \delta_n}\right]^T \\ &\approx \left[\frac{G_\delta\left(\boldsymbol{\delta}+h\mathbf{e}_1\right)-G_\delta\left(\boldsymbol{\delta}\right)}{h} \quad \frac{G_\delta\left(\boldsymbol{\delta}+h\mathbf{e}_2\right)-G_\delta\left(\boldsymbol{\delta}\right)}{h} \quad \cdots \right. \\ &\quad \left. \frac{G_\delta\left(\boldsymbol{\delta}+h\mathbf{e}_n\right)-G_\delta\left(\boldsymbol{\delta}\right)}{h}\right]^T,\end{aligned} \tag{39}$$

where, $\mathbf{e}_i, i = 1, 2, \ldots, n$ indicates the unit vector along ith dimension, and h is a small number.

3.3. Benchmark

Consider a performance function $G(\mathbf{x}) = (x_1 - 1)^2 + (x_2 - 2)^2 - 4$, with two uncertain variables $x_i = [-1, 1], (i = 1, 2)$. The uncertainty measure index can be expressed as

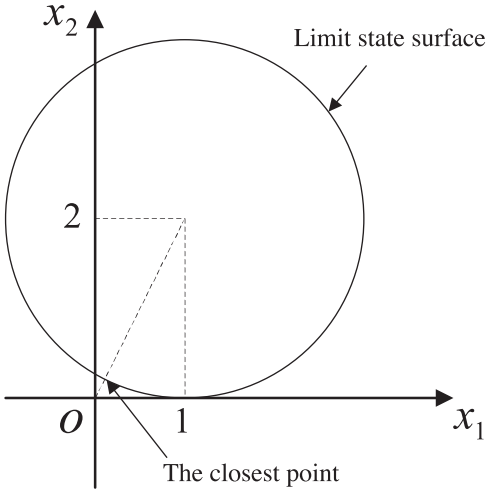

Fig. 4. Limit state surface and solution.

$$\begin{aligned}&\eta = \operatorname{sgn}(G(0)) \cdot \min\left(\|\mathbf{x}\|_\infty\right) \\ &s.t. \quad (x_1 - 1)^2 + (x_2 - 2)^2 - 4 = 0.\end{aligned} \tag{40}$$

The tolerance for both variables and object function are set to 0.1. The optimum solved by steepest descent method is $\bar{\boldsymbol{x}} = [0.1052 \quad 0.2107]^T$, and the constraint function value is 0.002276. By using the SAUA method, the optimum is $\mathbf{x}^* = [0.1055 \quad 0.2112]^T$, and the corresponding constraint function value is 2.48e−7. The exact solution of this problem is $\mathbf{x} = [0.1056 \quad 0.2111]^T$. The shape of limit state surface and the solution are shown in Fig. 4.

As a comparison, a classical optimization method – simplex method, and a surrogate assisted optimization – High Dimensional Model Representation (HDMR) based genetic algorithm (GA) are also used to solve this problem. Theoretically, any surrogate assisted optimization, such as radial basis function (RBF), Kriging, moving least square (MLS) methods, can be utilized to test the performance in this study. HDMR is recently developed surrogated modeling method. Compared with these method, HDMR is recently developed surrogated modeling method, the most attractive distinctive characteristic is that the highly accurate model can be achieved with the limited samples [65,66] and can be easily integrated with evolutionary algorithms [67]. Moreover, the distribution of the initial samples dose not influence the accuracy of the surrogate [66,68,69], it makes the comparison more representative and objective. Therefore, an alternative HDMR modeling method, Kriging based HDMR modeling [68] is selected for test and this

Table 1
Comparison of the performance of different methods for benchmark.

Algorithm	Number of evaluations	Optimal solution	Constraint function	Wall time/s
SAUA	65	(0.1055,0.2112)	2.48E−07	0.0475
Simplex	555	(0.1056,0.2111)	1.24E−07	0.0562
HDMR-GA	12	(0.1051,0.2113)	4.55E−04	70.1196

method has been proved to be an efficient and feasible for nonlinear problems. Additionally, since the accuracy of Kriging-HDMR can be guaranteed with the smaller size of samples, any evolutionary algorithm can be integrated with it. In this test, the GA is utilized due to its popularity. In our opinion, the performance of HDMR-GA is good enough to represent such a kind of methods.

The corresponding results are listed in Table 1. According to Table 1, the simplex method achieves a solution of highest accuracy with the constraint function value of 1.24e−07. While the HDMR assisted GA method shows the highest efficiency with 12 evaluations. The SAUA method reaches a trade-off between accuracy and efficiency, the accuracy is much higher than HDMR-GA and the efficiency is much higher than the simplex method. However, the SAUA is the most efficient one according to wall time criterion. Therefore, the SAUA method seems to achieve a solution of high accuracy with cheap computational cost.

4. The SAUA for material nonlinear problem integrated with reanalysis method

For a material nonlinear stiffness uncertainty analysis, Eq. (6) becomes

$$\eta = \mathrm{sgn}(G_\delta(0)) \cdot \min_{\boldsymbol{\delta}} \left(\|\boldsymbol{\delta}\|_\infty \right) \quad s.t. \quad G_\delta(\boldsymbol{\delta}) = u_s - u(\boldsymbol{\delta}) = 0 \tag{41}$$

where, $\boldsymbol{\delta}$ is uncertain variable, including material parameters, structural parameters and loads, and so on.u_s is the limit displacement.$u(\boldsymbol{\delta})$ is a displacement function, which is nonlinear, and usually solved by nonlinear FEM.

Since the performance function needs to be evaluated repeatedly, the uncertainty measure index is usually calculated by using surrogate instead of real evaluation. Although the efficiency can be significantly improved, the accuracy of the surrogate is difficult to be guaranteed, especially for nonlinear problems. To improve efficiency and accuracy simultaneously, an efficient RAMNA method is suggested. The method is based on pseudo elastic analysis and reanalysis method. The flowchart is shown in Fig. 5.

4.1. Incremental efficient material nonlinear analysis method

Sethuraman and Reddy developed a pseudo elastic analysis method for inelastic problems [70]. The elastoplastic deformation is described by using equivalent material parameters E_e and υ_e. The procedure of the elastoplastic analysis by using pseudo-elastic analysis method is described as follows:
Algorithm 1 ($\mathbf{F}$, σ_0, $\mathbf{d}$, $\boldsymbol{\varepsilon}$, $\boldsymbol{\sigma}$)

(1) Let $k=1$, $E_e^{(1)} = E$ and $\upsilon_e^{(1)} = \upsilon$, set δ to a small value.
(2) Calculate stiffness matrix $\mathbf{K}^{(k)}$ using $E_e^{(k)}$ and $\upsilon_e^{(k)}$.
(3) Solving the equation $\mathbf{K}^{(k)}\mathbf{d}^{(k)} = \mathbf{F}$ and calculate $\varepsilon^{(k)}$, $\boldsymbol{\sigma}^{(k)}$ and $\sigma_{eq}^{(k)}$.
(4) If $\sigma_{eq}^{(k)} < \sigma_0$, procedure goes to (7), otherwise, it goes to (5).
(5) Update E_e and υ_e for each element according to the corresponding material model.

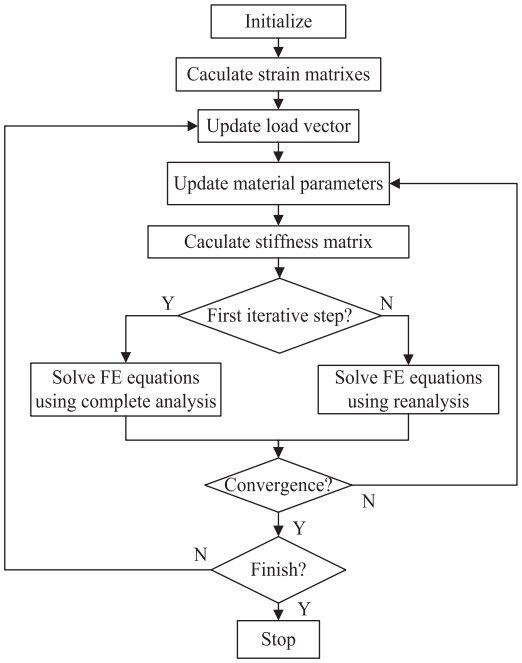

Fig. 5. Flowchart of RAMNA.

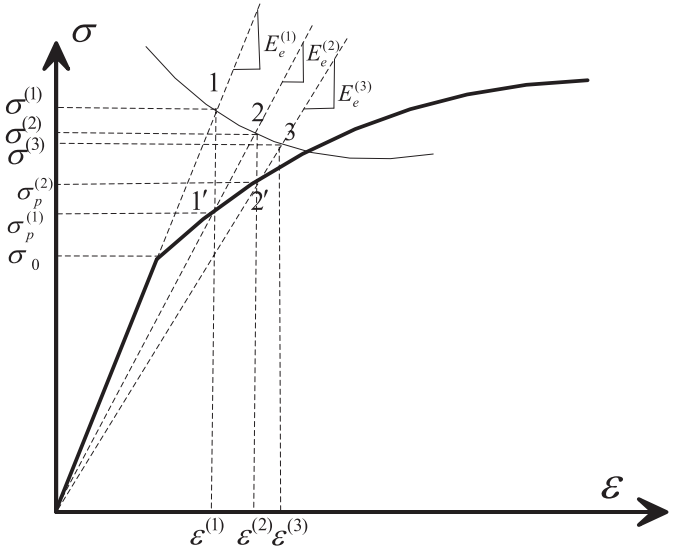

Fig. 6. Pseudo-elastic analysis.

(6) If $\sqrt{\frac{\sum_{i=1}^{N_{el}} (E_e^{k+1} - E_e^k)^2}{\sum_{i=1}^{N_{el}} E_e^k}} < \delta$, where N_{el} is the number of elements, $\sigma_0 = \sigma_{eq}^{(k)}$, procedure goes to (7), otherwise, $k=k+1$, it goes back to (2).
(7) $\mathbf{d} = \mathbf{d}^{(k)}$, $\boldsymbol{\varepsilon} = \boldsymbol{\varepsilon}^{(k)}$ and $\boldsymbol{\sigma} = \boldsymbol{\sigma}^{(k)}$, procedure stops.

The procedure is illustrated in Fig. 6.

The advantages of pseudo-elastic analysis method are that it can avoid calculating the complex elastoplastic constitutive matrix, and the convergence rate is almost the same as the NRM (Newton–Raphson method). This method is not widely used because it is based on total deformation theory, and it is not proper for the problems which are influenced by the loading path. To overcome this bottleneck, a pseudo-elastic analysis is extended to load increment method in this study.

Assuming that the stress and strain are obtained in the load step k as $\boldsymbol{\sigma}^{(k)}$ and $\varepsilon^{(k)}$. A load increment $\Delta\mathbf{F}^{(k)}$ is applied to the

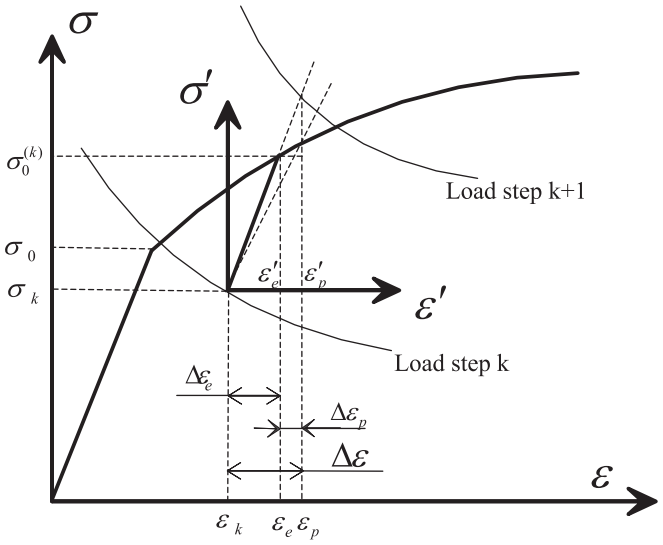

Fig. 7. Pseudo-elastic analysis for load increment method.

structure, and new stress $\boldsymbol{\sigma}^{(k+1)}$ and strain $\boldsymbol{\varepsilon}^{(k+1)}$ need to be resolved in the step $k+1$.

A transformation of coordinates for stress and strain is used to make the origin of the coordinates move to the current stress and strain as shown in Fig. 7. The transformation is

$$\begin{aligned}\boldsymbol{\sigma}' &= \Delta\boldsymbol{\sigma} = \boldsymbol{\sigma} - \boldsymbol{\sigma}^{(k)} \\ \boldsymbol{\varepsilon}' &= \Delta\boldsymbol{\varepsilon} = \boldsymbol{\varepsilon} - \boldsymbol{\varepsilon}^{(k)}.\end{aligned} \tag{42}$$

The current values of $\boldsymbol{\sigma}'$ and ε' are 0, therefore the pseudo-elastic theory developed for total strain theory can be used.

By using stress-strain curve, a simple strategy is proposed to calculate the equivalent elasticity modulus E_e.

As shown in Fig. 7, the initial stress-strain relation is assumed to be

$$\boldsymbol{\sigma} = f(\varepsilon). \tag{43}$$

It is easy to find that

$$E_e = \frac{E\Delta\varepsilon_e + f(\varepsilon_p) - f(\varepsilon_e)}{\Delta\varepsilon}. \tag{44}$$

For linear working hardening material, Eq. (44) becomes

$$E_e = \frac{E\Delta\varepsilon_e + E_T\Delta\varepsilon_p}{\Delta\varepsilon}. \tag{45}$$

The procedure of the load increment method using pseudo-elastic analysis is suggested as follows:

Algorithm 2

(1) Initially, $k=1$, $\mathbf{d}^{(k)}=0$, $\boldsymbol{\sigma}^{(k)}=0$, $\boldsymbol{\varepsilon}^{(k)}=0$ and $\sigma_0^{(k)}=\sigma_0$.
(2) Calculating $\Delta\mathbf{F}^{(k)}$.
(3) Algorithm 1 ($\Delta\mathbf{F}^{(k)}, \boldsymbol{\sigma}_0^{(k)}, \Delta\mathbf{d}^{(k)}, \Delta\boldsymbol{\varepsilon}^{(k)}, \Delta\boldsymbol{\sigma}^{(k)}$).
(4) $\mathbf{d}^{(k+1)}=\mathbf{d}^{(k)}+\Delta\mathbf{d}^{(k)}$, $\boldsymbol{\varepsilon}^{(k+1)}=\boldsymbol{\varepsilon}^{(k)}+\Delta\boldsymbol{\varepsilon}^{(k)}$, $\boldsymbol{\sigma}^{(k+1)}=\boldsymbol{\sigma}^{(k)}+\Delta\boldsymbol{\sigma}^{(k)}$ and $\sigma_0^{(k+1)}=\sigma_0^{(k)}$.
(5) $k=k+1$, if $k>N_{ls}$, where N_{ls} is the number of load steps, procedure goes to (6), otherwise it goes to (2).
(6) Procedure stops.

4.2. Efficient RAMNA method

In pseudo-elastic analysis, the load vector is fixed in each load step. While the change of the equivalent material parameters will lead to the change of stiffness matrix. If the problems are solved by complete analysis, large amount of computational cost will be expensive. Therefore, a reanalysis method, combined approximation (CA) [35,36], is employed to solve such problems efficiently.

Assume that the initial equilibrium equation of the structure is

$$\mathbf{K}_0\mathbf{d} = \mathbf{F}, \tag{46}$$

and the solution is $\mathbf{d}=\mathbf{d}_0$. After structural modifications or changes of the material parameters (the major issue discussed in this study), the equilibrium equation becomes

$$\mathbf{K}\mathbf{d} = \mathbf{F}. \tag{47}$$

The solution of Eq. (47) can be expressed as a linear combination of a series of vectors as

$$\mathbf{d} = \mathbf{v}_1 y_1 + \mathbf{v}_2 y_2 + \ldots + \mathbf{v}_s y_s = \mathbf{r}_B\mathbf{y}, \tag{48}$$

where $\mathbf{v}_i, i=1,2,\cdots,s$ are the basis vectors and $y_i, i=1,2,\cdots,s$ are the corresponding coefficients and s is the number of the basis vectors. In Eq. (48),

$$\begin{aligned}\mathbf{r}_B &= [\mathbf{v}_1 \quad \mathbf{v}_2 \cdots \mathbf{v}_s] \\ \mathbf{y} &= [y_1 \quad y_2 \cdots y_s]^T.\end{aligned} \tag{49}$$

The basis vectors can be calculated as follows:

$$\begin{aligned}\mathbf{v}_1 &= \mathbf{d}_0 \\ \mathbf{v}_i &= -\mathbf{B}\mathbf{v}_{i-1} (i=2,3,\ldots,s),\end{aligned} \tag{50}$$

where

$$\mathbf{B} = \mathbf{K}_0^{-1}\Delta\mathbf{K},\ \Delta\mathbf{K} = \mathbf{K} - \mathbf{K}_0. \tag{51}$$

Substitute Eq. (48) into Eq. (47) and pre-multiplying both side of Eq. (47) with $\mathbf{r}_B^T$, obtains

$$\mathbf{K}_R\mathbf{y} = \mathbf{F}_R, \tag{52}$$

where

$$\begin{aligned}\mathbf{K}_R &= \mathbf{r}_B^T\mathbf{K}\mathbf{r}_B \\ \mathbf{F}_R &= \mathbf{r}_B^T\mathbf{F}.\end{aligned} \tag{53}$$

Solve Eq. (52), $\mathbf{y}$ is obtained. By substituting $\mathbf{y}$ into Eq. (48), the approximation of $\mathbf{d}$ is achieved.

For each load step in load increment method, the material parameters used in the first iterative step are the same (elastic parameters). Therefore, the stiffness matrices are identical as well. The advantage is that the stiffness matrix needs to be decomposed only once, and it can be reused in all load steps for both initial analysis and CA. Theoretically, the CA has potential to improve the efficiency of pseudo-elastic analysis significantly. For this purpose, an efficient RAMNA method is proposed.

The procedure of the RAMNA is described as follows:

(1) Calculate elastic stiffness matrix $\mathbf{K}$ and the decomposition $\mathbf{K}=\mathbf{LU}$.
(2) For $k=1$ to N_{ls}
  Calculate the increment of the load vector $\Delta\mathbf{F}^{(k)}$.
  For $i=1$ to $N_{\max}$, where $N_{\max}$ is the largest number of iterative step
    If i equals to 1
      Solve $\mathbf{K}\mathbf{d}_i^{(k)}=\Delta\mathbf{F}^{(k)}$ using the decomposition $\mathbf{K}=\mathbf{LU}$
    Else
      Calculate elastoplastic stiffness matrix $\mathbf{K}_{ep}$
      Solve $\mathbf{K}_{ep}\mathbf{d}_i^{(k)}=\Delta\mathbf{F}^{(k)}$ using the CA method
    End if
    Update equivalent material parameters
    If convergence condition meets, break
  End for
  Update state variables
 End for
(3) Procedure stops.

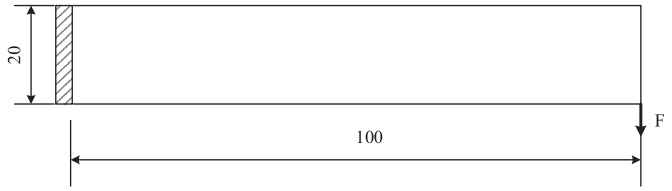

Fig. 8. Plane cantilever beam.

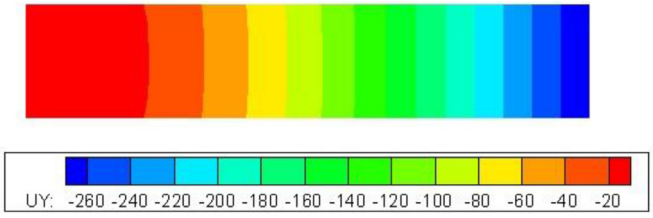

Self-developed program

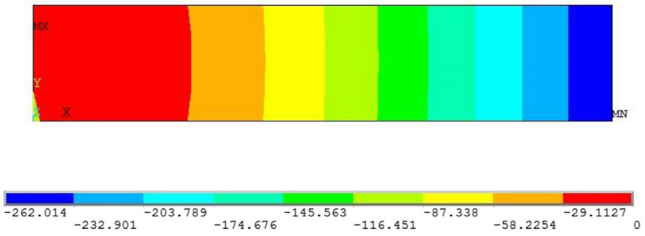

ANSYS

Fig. 9. Displacement along *x*-axis.

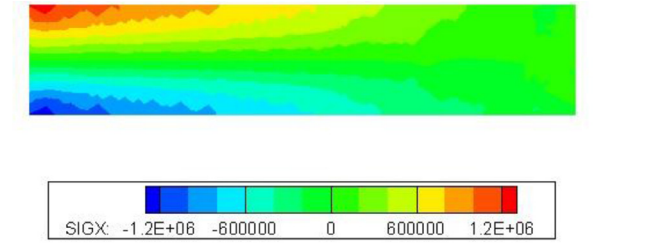

Self-developed program

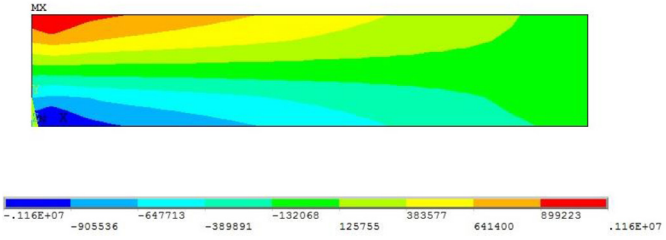

ANSYS

Fig. 10. Stress along *x*-axis.

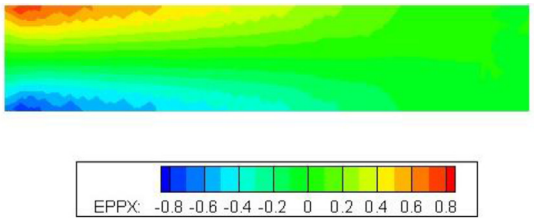

Self-developed program

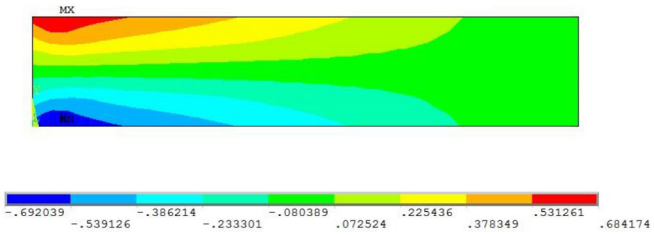

ANSYS

Fig. 11. Plastic strain along *x*-axis.

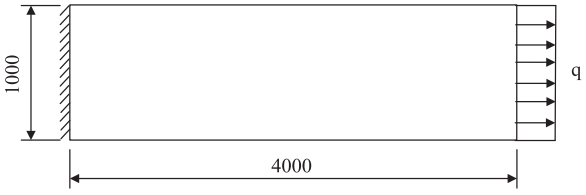

Fig. 12. Tensile plate.

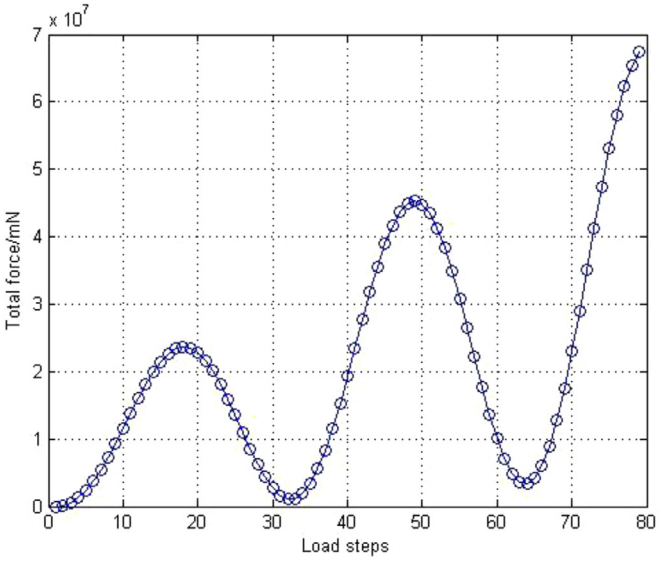

Fig. 13. Load steps.

4.3. Verification

(1) A plane cantilever beam is shown in Fig. 8. The left side of the beam is fixed, and a concentrate force is applied on the right side with value F = 1000 N. The material parameters are modulus of elasticity $E = 70$ GPa, Poisson's ratio of the material is $\upsilon = 0.3$, tangent modulus $E_T = 1.405$ GPa, yield limit $\sigma_Y = 120$ MPa. The structure is analyzed using self-coded program and a commercial software ANSYS, simultaneously. The results are shown in Figs. 9–11, which show that the self-developed program can obtain similar results to ANSYS.

(2) A plate and its size are shown in Fig. 12, and the thickness of the plate is $h = 10$ mm. The left side of the plate is fastened and a uniform force is implemented on the right side. The curve of the total value of the force is shown in Fig. 13. Linearly working hardening material is used in this example. The modulus of elasticity is $E = 70$ GPa, the Possion's ratio is $\nu = 0.3$, the yield limit is $\sigma_Y = 120$ MPa, and the tangent modulus is $E_T = 1.405$ GPa. The results obtained by complete analysis and approximate analysis are shown in Fig. 14. It is easy to observe that the result of complete analysis and approximate analysis are coincident. The error of stress be-

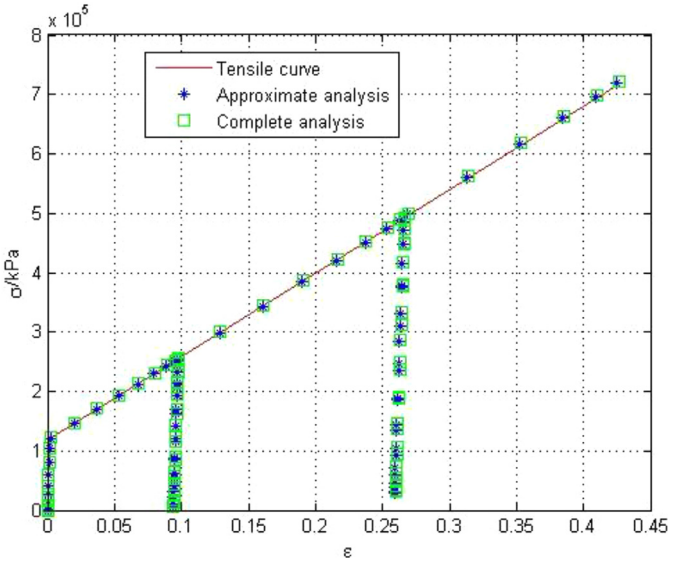

Fig. 14. Results of plate.

tween the two results is 1.17%, and the error of the strain is 1.20%.

5. Numerical examples

Three examples are shown in this section. The first case is presented to illustrate the application of analytic uncertainty analysis method for the elastic problem. The second and third cases are material nonlinear problems of vehicle parts, in which the SAUA method is used.

5.1. H-steel

An H-steel cantilever beam is shown in Fig. 15(a). The shape and size of cross section are shown in Fig. 15(b). The length of this beam is 1000 mm. The nodes of right side (marked B in Fig. 15(a)) are clamped, and a concentrated load is enforced on the center node of the left side (marked A in Fig. 15(a)) along the -z direction. The interval force is $F = 4000 \times (1 + \alpha\delta_1)$ N. The interval modulus of elasticity is $E = 70 \times (1 + \beta\delta_2)$ GPa. Different uncertain levels of force and modulus of elasticity (α and β) are concerned. Poisson's ratio is $\nu = 0.3$. The stiffness constraint is that the displacement of node A should be limited within 10 mm.

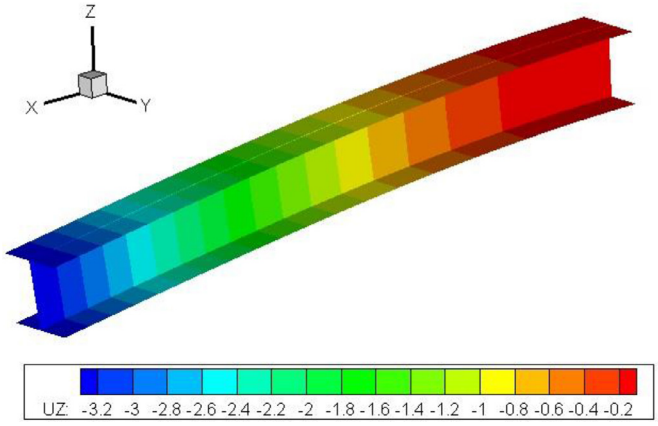

Fig. 16. Deformation of midpoint value.

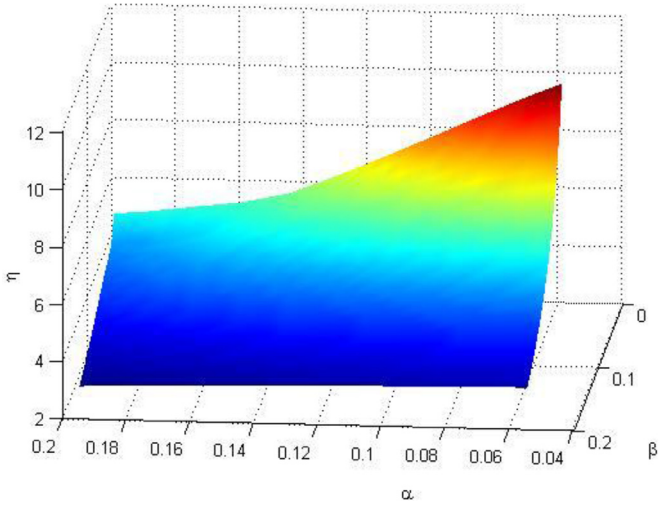

Fig. 17. Uncertainty of H-steel.

The deformation of midpoint value is shown in Fig. 16, and the uncertainty measure indexes are shown in Fig. 17 and corresponding results are listed in Table 2. Both α and β vary from 0.05 to

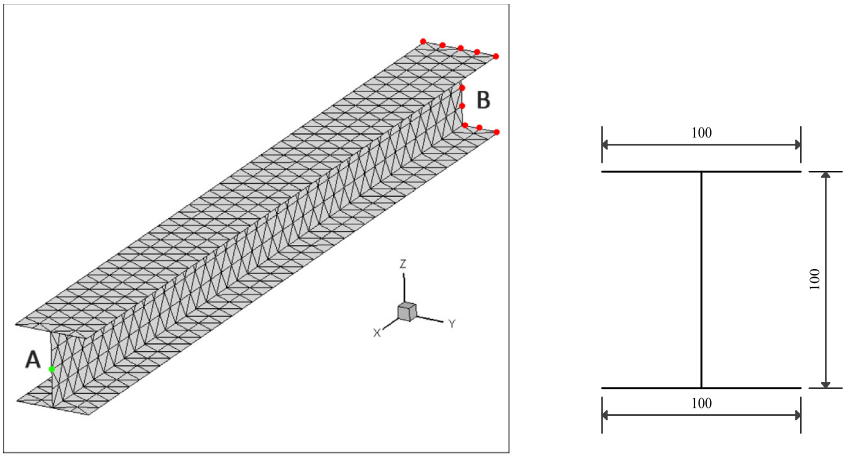

(a) H-steel (b) Cross section

Fig. 15. An illustration of H-steel model.

Table 2
Analytic reliability analysis result.

$\alpha\backslash\eta\backslash\beta$	0.050	0.065	0.080	0.095	0.110	0.125
0.050	11.7843	10.9905	10.1302	9.2558	8.4058	7.6052
0.065	9.4695	9.0648	8.6014	8.1015	7.5851	7.0686
0.080	7.8669	7.6368	7.3652	7.0620	6.7371	6.3997
0.095	6.7100	6.5679	6.3970	6.2022	5.9887	5.7613
0.110	5.8416	5.7480	5.6343	5.5029	5.3565	5.1980
0.125	5.1681	5.1034	5.0242	4.9317	4.8277	4.7137
0.140	4.6316	4.5851	4.5278	4.4606	4.3843	4.2999
0.155	4.1947	4.1602	4.1175	4.0672	4.0097	3.9458
0.170	3.8324	3.8061	3.7734	3.7348	3.6905	3.6410
0.185	3.5271	3.5067	3.4812	3.4509	3.4161	3.3770
0.200	3.2666	3.2503	3.2300	3.2059	3.1781	3.1468

$\alpha\backslash\eta\backslash\beta$	0.140	0.155	0.170	0.185	0.200
0.050	6.8676	6.5698	6.5070	6.4031	6.2711
0.065	6.5645	6.0817	5.6259	5.2001	5.0557
0.080	6.0575	5.7172	5.3840	5.0618	4.7533
0.095	5.5247	5.2832	5.0404	4.7996	4.5631
0.110	5.0301	4.8556	4.6768	4.4960	4.3151
0.125	4.5914	4.4626	4.3288	4.1915	4.0521
0.140	4.2087	4.1115	4.0095	3.9038	3.7952
0.155	3.8761	3.8014	3.7223	3.6396	3.5540
0.170	3.5868	3.5283	3.4660	3.4004	3.3320
0.185	3.3341	3.2875	3.2377	3.1849	3.1297
0.200	3.1122	3.0746	3.0342	2.9913	2.9461

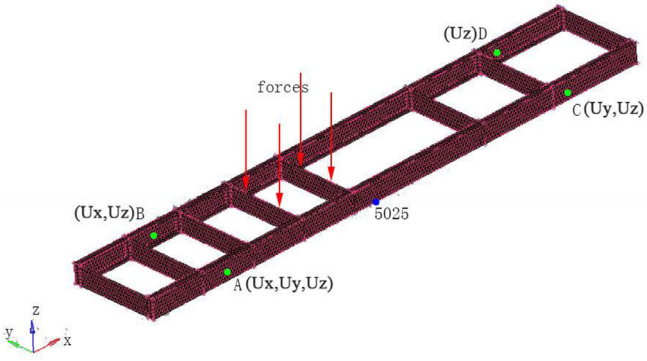

Fig. 18. Truck frame model.

Table 3
Uncertain variables of truck frame.

Uncertain variables	Interval expression
Force	$F = 15000 \times (1 + 0.05\delta_1)$ N
Elasticity modulus	$E = 70 \times (1 + 0.05\delta_2)$ GPa
Tangent modulus	$E_T = 1.405 \times (1 + 0.1\delta_3)$ GPa
Yield limit	$\sigma_Y = 120 \times (1 + 0.1\delta_4)$ MPa

0.2, and the uncertainty measure index η varies from 2.9461 to 11.7843. Since the values of η are larger than 1, the H-steel is reliable under such circumstance.

It should be noted that the FE analysis is carried out only once in the process of calculating the uncertainty measure index by analytic uncertainty analysis method. The analysis process is efficient.

5.2. Truck frame

A truck frame model, as well as the boundary conditions, is considered as shown in Fig. 18. The model includes 9752 elements and 5344 nodes, involving 32,064 degrees of freedom (DOFs). The uncertain variables are listed in Table 3 and all the uncertain variables are independently. The Poisson's ratio of the material is $\upsilon = 0.3$. The stiffness constraint is that the displacement of Node 5025 (as shown in Fig. 18) should be limited within 20 mm.

Table 4
Optimal results for truck frame.

Algorithm	Number of evaluations	Optimal solution	Constraint function
SAUA	161	(1.9514,0.0393,0.1785,1.8766)	−1.12e−4
HDMR-GA	36	(1.7690,1.4159,1.5423,1.7690)	−2.71e−1

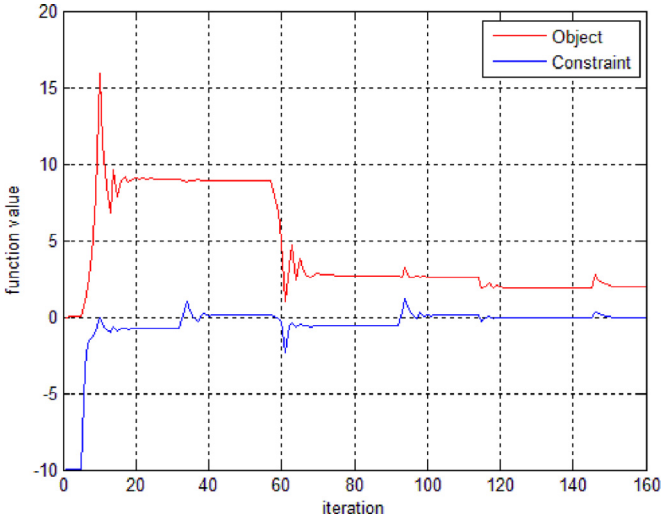

Fig. 19. Convergence curves of SAUA.

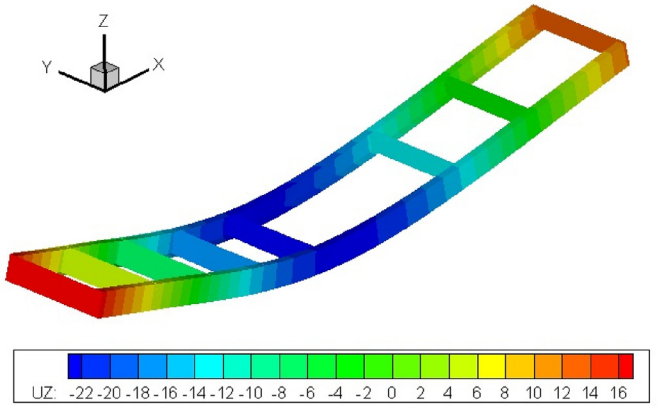

Fig. 20. Deformation of truck frame.

For the complete FE analysis and the suggested RAMNA, the computational costs of a single run are 215.567 s and 127.587 s, respectively. Obviously, the efficiency of the suggested method is about twice as FE analysis.

The optimal results of the SAUA and the HDMR-GA methods are listed in Table 4. Although the HDMR-GA has a small number of evaluations, the optimal solution does not satisfy the constraint function with value of −2.71e−1. The SAUA method achieves a feasible solution with a constraint function value of −1.12e−04, and the number of function evaluations is acceptable. The process does not converge based on the simplex method. The convergence curve of the SAUA method is shown in Fig. 19. According to the SAUA method, the uncertainty measure index is −1.9514, which indicates the structure is not reliable. The deformation of the optimal solution is shown in Fig. 20.

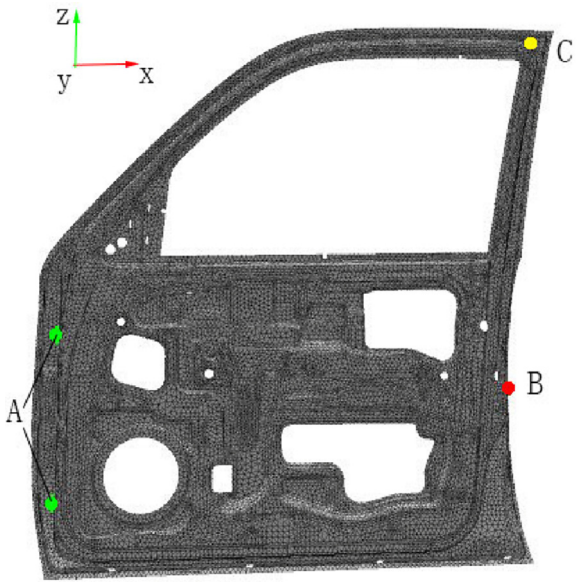

Fig. 21. Inner panel of car door.

Table 5
Uncertain variables of inner door panel.

Uncertain variables	Interval expression
Force	$F = 100 \times (1 + 0.05\delta_1)$N
Plasticity modulus	$E = 70 \times (1 + 0.05\delta_2)$GPa
Tangent modulus	$E_T = 1.405 \times (1 + 0.1\delta_3)$GPa
Yield limit	$\sigma_Y = 120 \times (1 + 0.1\delta_4)$MPa

Table 6
Optimal results for inner panel.

Algorithm	Number of evaluations	Optimal solution	Constraint function
SAUA	170	(0.5003,0.0783,0.0847,0.5219)	−2.65e−4
HDMR-GA	55	(0.3234,0.3234,0.2706,0.3233)	1.50e−1

5.3. Inner panel of car door

An inner panel of a car door is shown in Fig. 21. The model includes 35,308 elements and 18,243 nodes, involving 109,458 DOFs. For the nodes marked *A*, three translational DOFs are constrained. For a node marked *B*, the translational DOF along *y* direction is constrained, and a concentrated force is enforced along *–z* direction. The uncertain variables are listed in Table 5, and all the uncertain variables are independent. The Poisson's ratio of the material is $\upsilon = 0.3$. The stiffness requirement is that the displacement of the node marked *C* should be limited in 10 mm.

For the proposed RAMNA and complete analysis, the computational costs of a single run are 13.899 s and 28.688 s, respectively. The efficiency of the proposed method is over twice as FE analysis.

The optimal results of SAUA method and HDMR-GA method are listed in Table 6. The number of evaluations of HDMR-GA method is 55, which is much smaller than 170 of the SAUA method. However, the constraint function value of the HDMR-GA method is 1.50e−1. The optimal solution does not satisfy the constraint function. The SAUA method achieves a feasible solution with a constraint function value of −2.65e−4. The process does not converge based on the simplex method. The convergence curve of the SAUA method is shown in Fig. 22. According to the SAUA method, the uncertainty measure index is 0.5219, meaning the structure is unreliable. The deformation of the optimal solution is shown in Fig. 23.

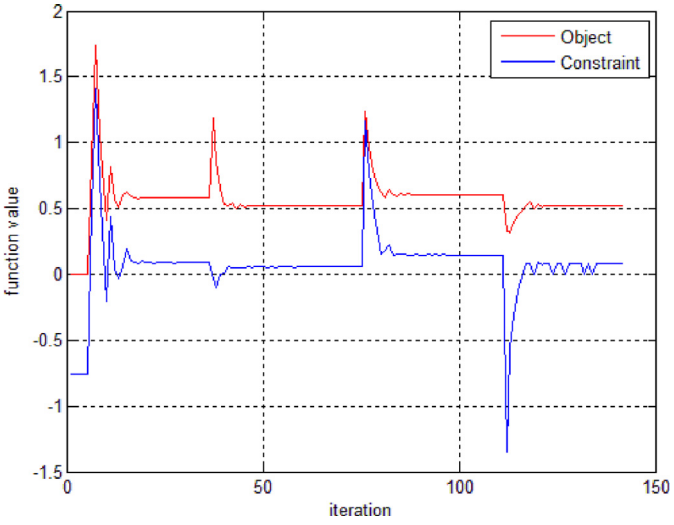

Fig. 22. Convergence curves of SAUA.

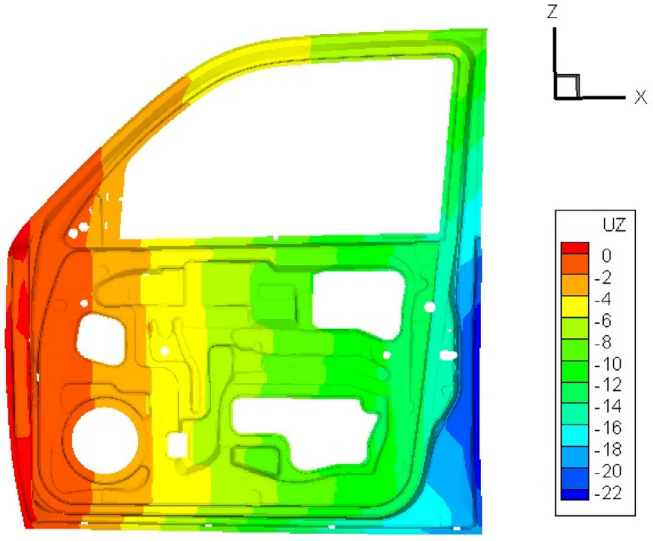

Fig. 23. Deformation of inner door panel.

6. Conclusions

This work suggests an efficient interval uncertainty analysis method for material nonlinear problems. Compared with other interval uncertainty analysis methods, the distinctive characteristics of this method can be summarized as:

(1) The formulations of an analytic uncertainty analysis for linear problems are proposed. The numerical example shows that the analytic method can calculate the uncertainty measure index efficiently.
(2) To extend the analytic interval method to nonlinear problems, a novel SAUA method is developed. The SAUA method is a combination of gradient-based optimization method and Taylor expansion. At the beginning of optimization, gradient-based optimization method is used to obtain a pseudo solution with a relax convergence criterion. Then the Taylor expansion is used when the optimization converges to a small region. In this way the optimization problem can be solved analytically. The numerical examples

show that the SAUA method can reach a trade-off between efficiency and accuracy. A highly accurate solution can be achieved efficiently via the SAUA method.

(3) An efficient RAMNA method is proposed. Compared with surrogate-based optimization and real evaluation, the accuracy and efficiency of suggested strategy can be promised simultaneously.

In conclusion, the proposed SAUA method is effective and efficient, which can contribute to shortening the period of structure design.

Acknowledgments

This work has been supported by Project of the Program of National Natural Science Foundation of China under the Grant Numbers 11572120, 11302266 and 61232014.

References

[1] Doltsinis I. Inelastic deformation processes with random parameters – methods of analysis and design. Comput Methods Appl Mech Eng 2003;192:2405–23.
[2] Liu B, Iwamura K. Modelling stochastic decision systems using dependent-chance programming. Eur J Oper Res 1997;101:193–203.
[3] Cho G. Log-barrier method for two-stage quadratic stochastic programming. Appl Math Comput 2005;164:45–69.
[4] Doltsinis I, Kang Z. Perturbation-based stochastic FE analysis and robust design of inelastic deformation processes. Comput Method Appl Mech Eng 2006;195:2231–51.
[5] Zhou D, Sun Y. The principle, method and calculation program of computer stochastic simulation. Wuhan: Huazhong University of science press; 1998.
[6] Jang H, Kim J, Lee J. Radiological risk assessment for field radiography based on two dimensional Monte Carlo analysis. Appl Radiat Isot 2009;67:1521–5.
[7] Ali T, Boruah H, Dutta P. Modeling uncertainty in risk assessment using double Monte Carlo method. Int J Eng and Innov Technol 2012;1:114–18.
[8] Ghanem RG, Spanos PD. Stochastic finite elements: a spectral approach. New York: Springer-Verlag New York Inc.; 1991.
[9] Herrera F, Verdegay JL. Three models of fuzzy integer linear programming. Eur J Oper Res 1995;83:581–93.
[10] Rommelfanger H. Fuzzy linear programming and applications. Eur J Oper Res 1996;92:512–27.
[11] Utkin LV, Gurov SV. A general formal approach for fuzzy reliability analysis in the possibility context. Fuzzy Sets Syst 1996;83:203–13.
[12] Yadav OP, Singh N, Chinnam RB, Goel PS. A fuzzy logic based approach to reliability improvement estimation during product development. Reliab Eng Syst Safety 2003;80:63–74.
[13] Jiang Q, Chen C. A numerical algorithm of fuzzy reliability. Reliab Eng Syst Safety 2003;80:299–307.
[14] Wu H. Bayesian system reliability assessment under fuzzy environment. Reliab Eng Syst Safety 2004;83:277–86.
[15] Ben-Haim Y. Convex models of uncertainty: applications and implications. Erkenntnis 1994;41:139–56.
[16] Ben-Haim Y. Convex models of uncertainty in radial pulse buckling of shells. J Appl Mech 1993;60:683–8.
[17] Pantelides CP. Stability of elastic bars on uncertain foundations using a convex model. Int J Solids Struct 1996;33:1257–69.
[18] Qiu Z, Ma L, Wang X. Ellipsoidal-bound convex model for the non-linear buckling of a column with uncertain initial imperfection. Int J of Non-Linear Mech 2006;41:919–25.
[19] Qiu Z, Elishakoff I. Antioptimization of structures with large uncertain-but-non-random parameters via interval analysis. Comput Methods Appl Mech Eng 1998;152:361–72.
[20] Sengupta A, Pal TK, Chakraborty D. Interpretation of inequality constraints involving interval coefficients and a solution to interval linear programming. Fuzzy Sets Syst 2001;119:129–38.
[21] Guo S, Lü Z. Interval arithmetic and static interval finite element method. Appl Math Mech 2001;22:1390–6.
[22] Jiang C, Han X, Liu G. Optimization of structures with uncertain constraints based on convex model and satisfaction degree of interval. Comput Methods Appl Mech Eng 2007;196:4791–800.
[23] Jiang C, Han X, Liu G, Li G. The optimization of the variable binder force in U-shape forming with uncertain friction coefficient. J Mater Process Technol 2007;182:262–7.
[24] Jiang C, Han X, Liu G. Uncertain optimization of composite laminated plates using a nonlinear interval number programming method. Comput Struct 2008;86:1696–703.
[25] Jiang C, Han X, Liu G. A sequential nonlinear interval number programming method for uncertain structures. Comput Methods Appl Mech Eng 2008;197:4250–65.
[26] Wu J, Luo Z, Zhang Y, Zhang N, Chen L. Interval uncertain method for multibody mechanical systems using CHebyshev inclusion functions. Int J Numer Meth Eng 2013;95:608–30.
[27] Li F, Luo Z, Sun G, Zhang N. An uncertain multidisciplinary design optimization method using interval convex models. Eng Optim 2012;45:1–23.
[28] Tuckeman LS. Divergence-free velocity fields in nonperiodic geometries. J Comput Phys 1989;80:403–41.
[29] Sherman J, Morrison WJ. Adjustment of an inverse matrix corresponding to changes in the elements of a given column or a given row of the original matrix. Ann Math Stat 1949;20(4):621.
[30] M. Woodbury. Inverting modified matrices. Memorandum Report, 42. Statistical Research Group. Princeton University, Princeton.
[31] Akgün MA, Garcelon JH, Haftka RT. Fast exact linear and non-linear structural reanalysis and the Sherman–Morrison–Woodbury formulas. Int J Numer Meth Eng 2001;50:1587–606.
[32] Cheikh M, Loredo A. Static reanalysis of discrete elastic structures with reflexive inverse. Appl Math Modell 2002;26:877–91.
[33] Huang G, Wang H, Li G. A reanalysis method for local modification and the application in large-scale problems. Struct Multidisc Optim 2014;49:915–30.
[34] Song Q, Chen P, Sun S. An exact reanalysis algorithm for local non-topological high-rank structural modifications in finite element analysis. Comput Struct 2014;143:60–72.
[35] Kirsch U. Combined approximations – a general reanalysis approach for structural optimization. Struct Multidisc Optim 2000;20:97–106.
[36] Kirsch U, Papalambros PY. Structural reanalysis for topological modifications – a unified approach. Struct Multidisc Optim 2001;21:333–44.
[37] Kirsch U. A unified reanalysis approach for structural analysis, design, and optimization. Struct Multidisc Optim 2003;25:67–85.
[38] Kirsch U, Moses F. An improved reanalysis method for grillage-type structures. Comput Struct 1998;68:79–88.
[39] Kirsch U, Papalambros PY. Exact and accurate reanalysis of structures for geometrical changes. Eng Comput 2001;17:363–72.
[40] Rong F, Chen S, Chen Y. Structural modal reanalysis for topological modifications with extended Kirsch method. Comput Methods Appl Mech Eng 2003;192:697–707.
[41] Kirsch U, Bogomolni M, Sheinman I. Nonlinear dynamic reanalysis of structures by combined approximations. Comput Methods Appl Eng 2006;195:4420–4432.
[42] Chen S, Yang Z. A universal method for structural static reanalysis of topological modification. Int J Numer Meth Eng 2004;61:673–86.
[43] Gao G, Wang H, Li G. An adaptive time-based global method for dynamic reanalysis. Struct Multidisc Optim 2013;48:355–65.
[44] Zhang G, Nikolaidis E, Mourelatos ZP. An efficient re-analysis methodology for probabilistic vibration of large-scale structures. J Mech Des 2009;131:1–13.
[45] Zuo W, Xu T, Zhang H, Xu T. Fast structural optimization with frequency constraints by genetic algorithm using adaptive eigenvalue reanalysis methods. Struct Multidisc Optim 2011;43(6):799–810.
[46] Zuo W, Bai J, Yu J. Sensitivity reanalysis of static displacement using Taylor series expansion and combined approximate method. Struct Multidisc Optim 2016;53(5):953–9.
[47] Sun R, Liu D, Xu T, Zuo W. New adaptive technique of kirsch method for structural reanalysis. AIAA J 2011;52(3):486–95.
[48] Zuo W, Yu Z, Zhao S, Zhang W. A hybrid Fox and Kirsch's reduced basis method for structural static reanalysis. Struct Multidisc Optim 2012;46(2):261–72.
[49] Yang Z, Chen X, Kelly R. An adaptive static reanalysis method for structural modifications using epsilon algorithm. Comput Sci Optim 2009;2:897–9.
[50] Chen S, Ma L, Meng G. Dynamic response reanalysis for modified structures under arbitrary excitation using epsilon-algorithm. Comput Struct 2008;86:2095–101.
[51] Kirsch U, Kocvara M, Zowe J. Accurate reanalysis of structures by a preconditioned conjugate gradient method. Int J Numer Meth Eng 2002;55:233–51.
[52] Wu B, Lim C, Li Z. A finite element algorithm for reanalysis of structures with added degrees of freedom. Finite Elem Anal Des 2004;40:1791–801.
[53] Wu B, Li Z. Reanalysis of structural modifications due to removal of degrees of freedom. Acta Mech 2005;180:61–71.
[54] Wang H, Li E, Li G. A parallel reanalysis method based on approximate inverse matrix for complex engineering problems. J Mech Des 2013;135(8):081001.
[55] Wang H, Zeng Y, Li E, Gao G. "Seen Is Solution" a CAD/CAE integrated parallel reanalysis design system. Comput Meth Appl Mech Eng 2016;299:187–214.
[56] He G, Wang H, Li E, Huang G, Li G. A multiple-GPU based parallel independent coefficient reanalysis method and applications for vehicle design. Adv Eng Software 2015;85:108–24.
[57] Wu B, Li Z. Static reanalysis of Structures with added degrees of freedom. Commun Numer Meth Eng 2006;22:269–81.
[58] Yang X, Chen S, Wu B. Eigenvalue reanalysis of structures using perturbations and Padé approximation. Mech Syst Sig Process 2001;15(2):257–63.
[59] Yang X, Lian H, Chen S. An adaptive iteration algorithm for structural modal reanalysis of topological modifications. Commun Numer Meth Eng 2002;18:373–82.
[60] Wu B, Li Z, Li S. The implementation of a vector-value rational approximate method in structural reanalysis problems. Comput Methods Appl Mech Eng 2003;192:1773–84.
[61] Whitley D. A genetic algorithm tutorial. Stat Comput 1994;4:65–85.

[62] Kirkpatrick S. Optimization by simulated annealing: quantitative studies. J Stat Phys 1984;34:975–86.
[63] Dorigo M, Gambardella LM. Ant colony system: a cooperative learning approach to the traveling salesman problem. IEEE Trans Evol Comput 1997;1:53–66.
[64] Jones DR, Schonlau M, Welch WJ. Efficient global optimization of expensive black-box functions. J Global Optim 1998;13:455–92.
[65] Rabitz H, Alis ÖF. General foundations of high-dimensional model representations. J Math Chem 1999;25:197–233.
[66] Shan S, Wang GG. Metamodeling for high dimensional simulation-based design problems. J Mech Des 2010;132(5):051009.
[67] Li E, Wang H. An alternative adaptive differential evolutionary algorithm assisted by expected improvement criterion and cut-HDMR expansion and its application in time-based sheet forming design. Adv Eng Software 2016;97:96–107.
[68] Tang L, Li G, Wang H. Kriging-HDMR metamodeling technique for nonlinear problems. Chin J Theor Appl Mech 2011;43:780–4.
[69] Wang H, Tang L, Li G. Adaptive MLS-HDMR metamodeling techniques for high dimensional problems. Expert Syst Appl 2011;38:14117–26.
[70] Sethuraman R, Reddy CS. Pseudo elastic analysis of material non-linear problems using element free Galerkin method. J Chin Inst Eng 2004;27:505–16.